AIAA SciTech Forum
11–15 & 19–21 January 2021, VIRTUAL EVENT
AIAA Scitech 2021 Forum

10.2514/6.2021-0380

Flow Parameter Estimation Based on On-board Measurements of Air Vehicle Traversing Turbulent Flows

Hengye Yang* and Dongheng Jing†
Cornell University, Ithaca, NY, 14850

Vahid Tarokh‡
Duke University, Durham, NC, 27708

Gregory Bewley§ and Silvia Ferrari¶
Cornell University, Ithaca, NY, 14850

Inspired by principles from particle transport theory in fluid dynamics, we recently developed a new energy-efficient control approach via implicit model following (IMF) for air vehicles traversing turbulent flows. However, the control design requires prior knowledge of the vortex timescale of the turbulent flow. In this paper, we propose an approach to estimate the turbulent flow parameters based on noisy on-board measurements without prior knowledge of the exact flow conditions, and validate it on a two-dimensional cellular flow model. By sparse identification of nonlinear dynamics (SINDy), the nonlinear vehicle dynamics with wind effects introduced are approximated as a sparsely weighted combination of user-defined candidate functions. Accordingly, separate optimization problems are set up to determine the weights representing the active level of candidate functions in the unknown nonlinear dynamics. We then identify the flow parameters by analyzing the weights statistically. Finally, the ability of the proposed method to estimate the flow parameters, including the mean velocity, the vortex length scale and the vortex timescale, is demonstrated by testing the algorithms on different measurement data sets with various initial conditions and flow parameters. We show that this method can accurately estimate the flow parameters within a permissible range of error.

I. Nomenclature

w_x, w_y	=	horizontal and vertical flow velocity components
U_0	=	mean velocity of the cellular flow
L_w	=	vortex length scale of the cellular flow
τ_w	=	vortex timescale of the cellular flow
$\mathbf{x}$	=	vehicle state
$\dot{\mathbf{x}}$	=	vehicle state derivative
$\mathbf{n}$	=	process noise
$\mathbf{f}$	=	nonlinear vehicle dynamics
$\mathbf{T}$	=	constant thrust
τ	=	inertial response time of the vehicle
$\boldsymbol{\Theta}$	=	a user-defined library of all potential candidate functions
$\mathbf{W}$	=	weight matrix representing the active level of candidate functions
f_{cand}	=	candidate function
L_{cand}	=	candidate length scale

*PhD Student, Laboratory for Intelligent Systems and Controls (LISC), Sibley School of Mechanical and Aerospace Engineering, AIAA Student Member. Email: hy469@cornell.edu

†Master Student, Laboratory for Intelligent Systems and Controls (LISC), Sibley School of Mechanical and Aerospace Engineering, AIAA Non-Member. Email: dj348@cornell.edu

‡Professor, Department of Electrical and Computer Engineering, AIAA Non-Member. Email: vahid.tarokh@duke.edu

§Assistant Professor and Director, Bewley Applied Turbulence Laboratory (BATL), Sibley School of Mechanical and Aerospace Engineering, AIAA Non-member. Email: gpb1@cornell.edu

¶John Brancaccio Professor and Director, Laboratory for Intelligent Systems and Controls (LISC), Sibley School of Mechanical and Aerospace Engineering, AIAA Associate Fellow. Email: ferrari@cornell.edu

II. Introduction

Inspired by principles from particle transport theory [1] and related experiments with water droplets settling in air turbulence [2], we have recently developed a new control approach via implicit model following (IMF) for air vehicles traversing turbulent flows [3, 4]. This control design enables the vehicle to exploit beneficial flow structures in the closed loop, thereby reducing the cost of time and energy for the vehicle to traverse turbulent flows. However, the method requires prior knowledge of the vortex timescale of the turbulent flow. In this paper, we develop techniques to estimate the turbulent flow parameters, including the mean velocity, the vortex length scale and the vortex timescale, based on noisy on-board measurements of an air vehicle traversing turbulent flows.

Estimating the flow structures of wind [5] and ocean currents [6] helps to guarantee the safety, robustness and efficiency of vehicle navigation in highly turbulent environments. Researchers have already successfully estimated the velocity profiles of wind [7] and water fields [8] based on the vehicle's corresponding dynamic responses. Song [9] proposed a flow-aided path planning algorithm for unmanned underwater vehicle (UUV) navigation in turbulent ocean currents using the measured flow velocity data. To minimize the time or energy consumption of a path planner, beneficial flow structures are often intentionally taken advantage of, while disadvantageous flow structures are usually evaded by autonomous vehicles [10]. In addition, Waslander [11] developed a wind disturbance estimation algorithm for a quadcopter, and used the estimated data to optimize its position control system and compensate for the wind disturbances. However, most of these existing flow estimation approaches for wind and ocean currents focus primarily on computing the precise velocity components of fluctuating flows, which have large measurement errors and require high computational cost [12, 13].

Turbulent flow structures can be characterized by some key flow parameters, including the mean velocity, the vortex timescale and the vortex length scale [14]. In this paper, we develop a method to estimate these turbulent flow parameters, and validate it on a two-dimensional cellular flow model. However, this method can be potentially extended to more complicated turbulence models. Without prior information of the exact flow parametric model, the novelty of this work is to only estimate the key flow parameters by determining the weights that represent which candidate functions are active in the nonlinear equations via sparse identification of nonlinear dynamics (SINDy). To approximate an unknown dynamic model, SINDy is a computationally efficient approach that considers the unknown nonlinear function as a sparsely weighted combination of all potential user-defined candidate functions, such as constant, polynomial and trigonometric terms [15]. The weights are then determined by solving separate optimization problems [16]. Until now, good performance of SINDy has been demonstrated by identifying various classical ordinary differential equation (ODE) and partial differential equation (PDE) models in fluid dynamics, such as the Lorenz deterministic nonperiodic flow model [17] and the PDE model for the cylinder wake [18].

This paper is organized as follows. In Section III, relevant background knowledge on the cellular flow model and SINDy is introduced. The problem of estimating the flow parameters based on noisy on-board measurements of an air vehicle traversing cellular flows without prior knowledge of the exact flow parametric model is formulated in Section IV. Section V illustrates an approach to estimate the flow parameters via SINDy. In Section VI, the proposed method is validated on different measurement data sets with various initial conditions and flow parameters, and numerical simulation results are correspondingly presented. Finally, the conclusion and future work are discussed in Section VII.

III. Background on Cellular Flow Model and SINDy

In this paper, the flow parameter estimation algorithms via SINDy are validated on a two-dimensional cellular flow model. Using noisy on-board measurements of an air vehicle traversing a cellular flow, the flow parameters, including the mean velocity, the vortex length scale and the vortex time scale, can be estimated accurately. The cellular flow model is first introduced in Subsection A. Some background knowledge and regular procedure of SINDy are presented in Subsection B.

A. Cellular Flow Model

To validate the flow parameter estimation algorithms, we employ a two-dimensional cellular flow model containing arrays of eddies that periodically alternate in their direction of rotation [19]. As a simplified model of homogeneous turbulent flows, cellular flow model approximates many natural flow phenomena, such as Langmuir cells in water [20]

and convective cellular motions in cloud [21]. The two-dimensional cellular flow model can be expressed as

$$w_x = U_0 sin(\frac{\pi x}{L_w}) cos(\frac{\pi y}{L_w}) \tag{1a}$$

$$w_y = -U_0 cos(\frac{\pi x}{L_w}) sin(\frac{\pi y}{L_w}) \tag{1b}$$

where x and y represent the position in the world frame, w_x and w_y are the horizontal and vertical flow velocity components respectively, U_0 is the mean velocity, and L_w is the length scale of the cellular flow. The vortex timescale τ_w is defined as the vortex's turnover time, and is given by

$$\tau_w \equiv \frac{L_w}{U_0} \tag{2}$$

B. Sparse Identification of Nonlinear Dynamics (SINDy)

SINDy is a method that identifies an unknown nonlinear dynamical equation as a sparse combination of all potential user-defined candidate functions [16]. In general, we first consider a nonlinear dynamical equation of the form,

$$\dot{\mathbf{x}}(t) = \mathbf{f}[\mathbf{x}(t)], \ \mathbf{x}(t_0) = \mathbf{x}_0 \tag{3}$$

where $\mathbf{x} \in \mathbb{R}^n$ is the state of the dynamical system, $\mathbf{f}$ is a nonlinear function, and $\mathbf{x}_0$ is the initial condition. To sparsely identify the function $\mathbf{f}$ based on noisy on-board measurements, the state $\mathbf{x}$ and the state derivative $\dot{\mathbf{x}}$ are sampled at times $t_1, t_2, \cdots, t_m$, and then arranged into matrices, $\mathbf{X} \in \mathbb{R}^{m \times n}$ and $\dot{\mathbf{X}} \in \mathbb{R}^{m \times n}$, respectively,

$$\mathbf{X} = [\mathbf{x}(t_1) \ \ \mathbf{x}(t_2) \ \cdots \ \mathbf{x}(t_m)]^T \tag{4a}$$

$$\dot{\mathbf{X}} = [\dot{\mathbf{x}}(t_1) \ \ \dot{\mathbf{x}}(t_2) \ \cdots \ \dot{\mathbf{x}}(t_m)]^T \tag{4b}$$

We then construct a set of candidates $\mathbf{\Theta}(\mathbf{X}) \in \mathbb{R}^{m \times k}$ containing k user-defined candidate functions, each column of which represents the sampled values of the corresponding candidate function at times $t_1, t_2, \cdots, t_m$:

$$\mathbf{\Theta}(\mathbf{X}) = \Big[f_1(\mathbf{X}) \ \ f_2(\mathbf{X}) \ \cdots \ f_k(\mathbf{X}) \Big] \tag{5}$$

where the potential candidate functions are denoted as $f_i, \ i = 1, 2, \cdots, k$. After that, separate optimization problems can be set up to identify the relative importance of these candidate functions by determining the sparse coefficients in the weight matrix $\mathbf{W}$ [15]:

$$\dot{\mathbf{X}} = \mathbf{\Theta}(\mathbf{X})\mathbf{W} \tag{6}$$

where $\mathbf{W} \in \mathbb{R}^{k \times n}$ is the weight matrix representing the active level of candidate functions in the unknown nonlinear dynamics. Therefore, SINDy can determine the weight matrix $\mathbf{W}$ by solving optimization problems via linear regression, and approximate the nonlinear function $\mathbf{f}$ that maps the state $\mathbf{x}$ to the state derivative $\dot{\mathbf{x}}$ as a sparsely weighted linear combination of candidate functions.

IV. Problem Formulation

Given a thrust-driven air vehicle traversing a cellular flow with mean velocity U_0 and vortex length scale L_w, we consider the problem of estimating the flow parameters $\mathbf{p} = [U_0 \ L_w]^T$ from noisy flight data, including the vehicle state $\mathbf{x} \in \mathbb{R}^n$ and the vehicle state derivative $\dot{\mathbf{x}} \in \mathbb{R}^n$, collected at times $t_1, t_2, \cdots, t_m$ in the form,

$$\dot{\mathbf{x}}(t_i) = \mathbf{f}(\mathbf{x}(t_i); \mathbf{p}) + \mathbf{n}(t_i), \ i = 1, 2, \cdots, m \tag{7}$$

where the nonlinear function $\mathbf{f}$ represents the vehicle dynamics, and the process noise $\mathbf{n} \in \mathbb{R}^n$ is modeled as a vector of independent and identically distributed zero-mean Gaussian noise. In this paper, the vehicle state $\mathbf{x}$ is assumed to be fully measurable, and the state derivative $\dot{\mathbf{x}}(t)$ is then numerically estimated using finite difference approximation. If this assumption is not met and derivatives cannot be estimated using finite differences, an optimal on-board state

estimator can be used instead. Sampled vehicle states $\mathbf{x}$ and state derivatives $\dot{\mathbf{x}}$ at times $t_1, t_2, \cdots, t_m$ are then arranged into matrices, $\mathbf{X} \in \mathbb{R}^{m\times n}$ and $\dot{\mathbf{X}} \in \mathbb{R}^{m\times n}$, respectively.

Based on prior basic knowledge of the cellular flow characteristics, we construct a set of candidates $\boldsymbol{\Theta}(\mathbf{X}) \in \mathbb{R}^{m\times k}$ containing k user-defined candidate functions. The nonlinear vehicle dynamics $\mathbf{f}$ is then approximated as a sparsely weighted linear combination of all potential user-defined candidate functions:

$$\dot{\mathbf{X}} = \boldsymbol{\Theta}(\mathbf{X})\mathbf{W} + \mathbf{N} \tag{8}$$

where $\mathbf{W} \in \mathbb{R}^{k\times n}$ is the weight matrix representing the active level of candidate functions, and the noise $\mathbf{N} \in \mathbb{R}^{m\times n}$ is modeled as a matrix of independent and identically distributed zero-mean Gaussian noise. After that, we set up n separate optimization problems to identify the relative importance of these candidate functions by determining the sparse column vectors of coefficients $\mathbf{w}_j \in \mathbb{R}^k$ in the weight matrix $\mathbf{W}$:

$$\mathbf{w}_j = \underset{\mathbf{w}_j}{argmin} \|\dot{\mathbf{x}}_j - \boldsymbol{\Theta}(\mathbf{x}_j)\mathbf{w}_j\|_2^2, \ j = 1, 2, \cdots, n \tag{9}$$

where $\mathbf{x}_j$ and $\dot{\mathbf{x}}_j$ are the jth column of the sampled matrices $\mathbf{X}$ and $\dot{\mathbf{X}}$ respectively. The unknown vector of cellular flow parameters $\mathbf{p} = [U_0 \ L_w]^T$ can then be identified by analyzing the weights statistically based on prior knowledge of the cellular flow characteristics and vehicle dynamics. Here, we assume that the cellular flow parameters U_0 and L_w are both unknown bounded constants, so there exist a lower bound and an upper bound for both flow parameters.

V. Flow Parameter Estimation

The flow parameter estimation algorithms presented in this paper contain four essential steps: collecting the flight data from numerical simulations, constructing a set of potential candidate functions, solving sparse optimization problems to identify which candidate functions are active in the nonlinear dynamics, and estimating the flow parameters statistically. In this paper, the parameter estimation algorithms are developed and validated on an ideal point-mass thrust-driven air vehicle model introduced in Subsection A. The flight data are simulated according to this air vehicle model. Then, the procedure for constructing a set of potential candidate functions based on prior knowledge of the target problem is presented in Subsection B. Finally, in Subsection C, sparse optimization problems are set up to determine active candidate functions, and the flow parameters are then estimated statistically.

A. Air Vehicle Model and Flight Data Simulation

There is a significant precedent for treating autonomous vehicles, such as fixed-wing aircraft [22, 23], quadcopters [24, 25] and unmanned ground robots [26, 27], as point masses. In this work, the assumption of treating an air vehicle traversing a cellular flow as a point mass holds when the order of magnitude of the vehicle span L is much smaller than that of the vortex length scale L_w of the cellular flow. Inspired by the dynamics of spherical inertial particles [28], the two-dimensional governing equation for the dynamics of a thrust-driven point-mass air vehicle of mass m and span L takes the form,

$$m\dot{\mathbf{v}}(t) = -3\pi L\mu[\mathbf{v}(t) - \mathbf{w}(t)] + \mathbf{T} \tag{10}$$

where $\mathbf{v} \in \mathbb{R}^2$ is the velocity of the air vehicle, μ is the dynamic viscosity of surrounding fluid, $\mathbf{w} \in \mathbb{R}^2$ is the flow velocity, and $\mathbf{T} \in \mathbb{R}^2$ is a constant thrust. In this model, the air vehicle is subject to a linear Stokes drag force. This assumption holds when the flow is incompressible and the vehicle size is sufficiently small so that the Reynolds number for the vehicle traversing the flow is smaller than one. The inertial response time τ of the vehicle to changes in surrounding flow conditions is given by

$$\tau \equiv \frac{m}{3\pi L\mu} \tag{11}$$

Therefore, combining Eqns. 10 and 11, the ideal two-dimensional dynamic model of the point-mass air vehicle driven by a constant thrust can be rearranged as

$$\dot{\mathbf{v}}(t) = \frac{1}{\tau}[\mathbf{w}(t) - \mathbf{v}(t)] + \mathbf{a}_t \tag{12}$$

where $\mathbf{a}_t = \frac{1}{m}\mathbf{T} = [a_x \ a_y]^T$ is the acceleration produced by the constant thrust $\mathbf{T}$. Based on the cellular flow model in Eqn. 1, the flow velocity can be written as a periodic function $\mathbf{\Phi}$ of the vehicle's position x and y, given the flow parameters $\mathbf{p} = [U_0 \ L_w]^T$:

$$\mathbf{\Phi}(x, y; \mathbf{p}) = \begin{bmatrix} w_x \\ w_y \end{bmatrix} = U_0 \begin{bmatrix} f_1(x, y; L_w) \\ f_2(x, y; L_w) \end{bmatrix} \tag{13}$$

where $\mathbf{\Phi}$ is an unknown sparse function in the space of all potential candidate functions, and f_1 and f_2 are unknown periodic functions. Given that the maximum magnitude of the flow velocity cannot exceed U_0, the maximum amplitudes of f_1 and f_2 are both $\sqrt{2}/2$. Combining Eqns. 12 and 13, the dynamic model of a point-mass thrust-driven air vehicle with the inertial response time τ traversing a cellular flow with the mean velocity U_0 and vortex length scale L_w can be written in standard state-space form,

$$\dot{\mathbf{x}} = \begin{bmatrix} 0 & 0 & 1 & 0 \\ 0 & 0 & 0 & 1 \\ -\frac{1}{\tau} & 0 & 0 & 0 \\ 0 & -\frac{1}{\tau} & 0 & 0 \end{bmatrix} \mathbf{x} + \frac{U_0}{\tau} \begin{bmatrix} 0 \\ 0 \\ f_1(x, y; L_w) \\ f_2(x, y; L_w) \end{bmatrix} + \begin{bmatrix} 0 \\ 0 \\ a_x \\ a_y \end{bmatrix} \tag{14}$$

where $\mathbf{x} = [x \ y \ v_x \ v_y]^T \in \mathbb{R}^4$ is the state vector, and a_x and a_y are the horizontal and vertical components of the acceleration produced by constant thrust. In numerical simulations, the vehicle state $\mathbf{x}$ is collected at times $t_1, t_2, \cdots, t_{m+1}$, and the state derivative $\dot{\mathbf{x}}$ is then numerically estimated using finite difference approximation:

$$\dot{\mathbf{x}}(t_i) = \frac{\mathbf{x}(t_{i+1}) - \mathbf{x}(t_i)}{t_{i+1} - t_i}, \ i = 1, 2, \cdots, m \tag{15}$$

A more accurate alternative is to use an optimal estimator for the state derivative estimation, but this is also more computationally expensive. The vehicle states $\mathbf{x}$ and state derivatives $\dot{\mathbf{x}}$ collected at times $t_1, t_2, \cdots, t_m$ are then arranged into matrices, $\mathbf{X} \in \mathbb{R}^{m\times 4}$ and $\dot{\mathbf{X}} \in \mathbb{R}^{m\times 4}$, respectively:

$$\mathbf{X} = \begin{bmatrix} \mathbf{X}_1 & \mathbf{X}_2 & \mathbf{X}_3 & \mathbf{X}_4 \end{bmatrix} = \begin{bmatrix} x_1(t_1) & x_2(t_1) & x_3(t_1) & x_4(t_1) \\ x_1(t_2) & x_2(t_2) & x_3(t_2) & x_4(t_2) \\ \vdots & \vdots & \vdots & \vdots \\ x_1(t_m) & x_2(t_m) & x_3(t_m) & x_4(t_m) \end{bmatrix} \tag{16a}$$

$$\dot{\mathbf{X}} = \begin{bmatrix} \dot{\mathbf{X}}_1 & \dot{\mathbf{X}}_2 & \dot{\mathbf{X}}_3 & \dot{\mathbf{X}}_4 \end{bmatrix} = \begin{bmatrix} \dot{x}_1(t_1) & \dot{x}_2(t_1) & \dot{x}_3(t_1) & \dot{x}_4(t_1) \\ \dot{x}_1(t_2) & \dot{x}_2(t_2) & \dot{x}_3(t_2) & \dot{x}_4(t_2) \\ \vdots & \vdots & \vdots & \vdots \\ \dot{x}_1(t_m) & \dot{x}_2(t_m) & \dot{x}_3(t_m) & \dot{x}_4(t_m) \end{bmatrix} \tag{16b}$$

where $\mathbf{X}_i \in \mathbb{R}^m$ and $\dot{\mathbf{X}}_i \in \mathbb{R}^m$, $i = 1, 2, 3, 4$, are the sampled time histories of the four states and state derivatives respectively.

B. Candidate Functions

SINDy approximates the nonlinear equation as a sparsely weighted linear combination of user-defined candidate functions. As a fist step, we construct a group of candidate functions $\mathbf{\Theta}(\mathbf{X})$ based on prior basic knowledge of the target problem. As introduced in Section III, the vortex length scale L_w is defined as the vortex's turnover time in the cellular flow. Since the unknown equations f_1 and f_2 in Eqn. 13 are both periodic functions of position x and y in the world frame, the ultimate candidate function f_{cand} should be in the set of functions containing trigonometric terms with a period of $2L_w$ or the product of them:

$$f_{cand} \in \{\sin\frac{\pi x}{L_w}, \sin\frac{\pi y}{L_w}, \cos\frac{\pi x}{L_w}, \cos\frac{\pi y}{L_w}, \sin\frac{\pi x}{L_w}\sin\frac{\pi y}{L_w}, \sin\frac{\pi x}{L_w}\cos\frac{\pi y}{L_w}, \cos\frac{\pi x}{L_w}\sin\frac{\pi y}{L_w}, \cos\frac{\pi x}{L_w}\cos\frac{\pi y}{L_w}\} \tag{17}$$

Given that the vortex length scale L_w is a constant within the range from a lower bound L_{lb} to an upper bound L_{ub}, the ultimate candidate length scale L_{cand} should be in the following set containing all potential discretized length scales:

$$L_{cand} \in \{L_{lb}, L_{lb} + dL, L_{lb} + 2dL, \cdots, L_{ub}\} \tag{18}$$

where dL is the incremental length scale. After choosing candidate trigonometric functions and length scales, we can obtain the complete library of candidate functions $\mathbf{\Theta}(\mathbf{X})$ containing all potential candidates:

$$\mathbf{\Theta}(\mathbf{X}) = \begin{bmatrix} \sin(\frac{\pi}{L_{cand}}\mathbf{X}_1)^T \\ \sin(\frac{\pi}{L_{cand}}\mathbf{X}_2)^T \\ \cos(\frac{\pi}{L_{cand}}\mathbf{X}_1)^T \\ \cos(\frac{\pi}{L_{cand}}\mathbf{X}_2)^T \\ [\sin(\frac{\pi}{L_{cand}}\mathbf{X}_1) \otimes \sin(\frac{\pi}{L_{cand}}\mathbf{X}_2)]^T \\ [\sin(\frac{\pi}{L_{cand}}\mathbf{X}_1) \otimes \cos(\frac{\pi}{L_{cand}}\mathbf{X}_2)]^T \\ [\cos(\frac{\pi}{L_{cand}}\mathbf{X}_1) \otimes \sin(\frac{\pi}{L_{cand}}\mathbf{X}_2)]^T \\ [\cos(\frac{\pi}{L_{cand}}\mathbf{X}_1) \otimes \cos(\frac{\pi}{L_{cand}}\mathbf{X}_2)]^T \end{bmatrix}^T = \begin{bmatrix} \sin(\frac{\pi}{L_{lb}}\mathbf{X}_1)^T \\ \sin(\frac{\pi}{L_{lb}+dL}\mathbf{X}_1)^T \\ \vdots \\ \sin(\frac{\pi}{L_{ub}}\mathbf{X}_1)^T \\ \vdots \\ [\cos(\frac{\pi}{L_{lb}}\mathbf{X}_1) \otimes \cos(\frac{\pi}{L_{lb}}\mathbf{X}_2)]^T \\ [\cos(\frac{\pi}{L_{lb}+dL}\mathbf{X}_1) \otimes \cos(\frac{\pi}{L_{lb}+dL}\mathbf{X}_2)]^T \\ \vdots \\ [\cos(\frac{\pi}{L_{ub}}\mathbf{X}_1) \otimes \cos(\frac{\pi}{L_{ub}}\mathbf{X}_2)]^T \end{bmatrix}^T \tag{19}$$

where $\mathbf{X}_1 \in \mathbb{R}^m$ and $\mathbf{X}_2 \in \mathbb{R}^m$ are the sampled time histories of the vehicle position x and y at times $t_1, t_2, \cdots, t_m$ respectively, and the symbol $\otimes$ represents element-wise multiplication. Each column of $\mathbf{\Theta}(\mathbf{X})$ represents the sampled values of the corresponding candidate function at times $t_1, t_2, \cdots, t_m$. In Eqn. 19, each type of trigonometric candidate functions corresponds with the same number of elements as the set of all potential discretized length scales. For convenience, in the next subsection, the ith trigonometric candidate function in Eqn. 17 is denoted as $f_{cand,i}$, and the jth candidate length scale in Eqn. 18 is denoted as $L_{cand,j}$. It should be noted that choosing the range of L_{cand} and the incremental length scale dL is essential, because the size of candidate function set $\mathbf{\Theta}(\mathbf{X})$ cannot exceed the length of measurement data set in order to make the formulated optimization problems solvable.

C. Optimization and Parameter Estimation

Given the user-defined candidate function set $\mathbf{\Theta}(\mathbf{X})$, we set up n separate optimization problems to identify the relative importance of these candidate functions by determining the sparse column vectors of coefficients $\mathbf{w}_j$ in the weight matrix $\mathbf{W}$ via least squares [16]:

$$\mathbf{w}_j = \underset{\mathbf{w}_j}{argmin} \|\dot{\mathbf{x}}_j - \mathbf{\Theta}(\mathbf{x}_j)\mathbf{w}_j\|_2^2, \ j = 1, 2, \cdots, n \tag{20}$$

where $\mathbf{x}_j$ and $\dot{\mathbf{x}}_j$ are the jth column of the sampled matrices $\mathbf{X}$ and $\dot{\mathbf{X}}$ respectively. Each element of $\mathbf{W}$, denoted as $w(f_{cand,i}, L_{cand,j})$, corresponds with the ith candidate function and the jth candidate length scale. Then, all weights corresponding to a certain $L_{cand,j}$ are summed up, and the estimated length scale $\hat{L}_w$ is the candidate length scale with the highest weight sum:

$$\hat{L}_w = \underset{L_{cand,j}}{argmax} \sum_i w(f_{cand,i}, L_{cand,j}) \tag{21}$$

Given the ultimate goal to estimate the flow parameters U_0 and L_w, it is not necessary to identify the exact form of periodic functions f_1 and f_2. After obtaining the estimated length scale $\hat{L}_w$, we update the set of candidate functions accordingly. The updated set of candidates, denoted as $\mathbf{\Theta}^*$, contains all periodic candidate functions with $\hat{L}_w$ only. Therefore, the size of the updated candidate set $\mathbf{\Theta}^*$ is significantly smaller than that of the original $\mathbf{\Theta}$. Using SINDy, we can obtain the expected periodic functions, denoted as $\bar{f}_1$ and $\bar{f}_2$, by calculating the weighted sum of all periodic candidate functions with non-zero weights. Given that the maximum magnitude of the flow velocity cannot exceed U_0, the maximum amplitudes of identified f_1 and f_2 should both be $\sqrt{2}/2$. Hence, both expected periodic functions $\bar{f}_1$ and $\bar{f}_2$ have to be normalized to meet this requirement:

$$f_i^* = \sqrt{2} \cdot \frac{\bar{f}_i - \frac{1}{2}[max(\bar{f}_i) + min(\bar{f}_i)]}{max(\bar{f}_i) - min(\bar{f}_i)}, \ i = 1, 2 \tag{22}$$

where f^* is the normalized periodic function, and $\bar{f}$ is the expected periodic function. Plugging the normalized periodic function $\mathbf{f}^* = [f_1^* \ f_2^*]^T$ back in Eqn. 13, we can obtain the flow velocity components in the form,

$$\mathbf{\Phi}(\mathbf{X}) = U_0 \mathbf{f}^*(\mathbf{X}) \tag{23}$$

where $\mathbf{X}$ contains sampled vehicle states, and $\mathbf{\Phi}(\mathbf{X})$ is obtained from sampled vehicle state derivatives based on prior basic knowledge of the cellular flow characteristics and the vehicle dynamics in Eqn. 14. Then, U_0 can be estimated by averaging the coefficients in front of the normalized periodic function $\mathbf{f}^*(\mathbf{X})$:

$$\hat{U}_0 = \langle \mathbf{\Phi}(\mathbf{X}) [\mathbf{f}^*(\mathbf{X})]^{-1} \rangle \tag{24}$$

Given the estimated mean velocity $\hat{U}_0$ and vortex length scale $\hat{L}_w$, the estimated vortex timescale $\hat{\tau}_w$ can then be calculated:

$$\hat{\tau}_w = \frac{\hat{L}_w}{\hat{U}_0} \tag{25}$$

VI. Numerical Results

In numerical simulations, the ability of the presented method to estimate the mean velocity U_0, the vortex length scale L_w and the vortex timescale τ_w of the cellular flow is demonstrated by testing the algorithms on different simulated data sets with various flow parameters and initial conditions. First, the performance of parameter estimation algorithms is validated on a simulated air vehicle traversing a cellular flow with the mean velocity $U_0^* = 15.43m/s$, the vortex length scale $L_w^* = 4.21m$ and the vortex timescale $\tau_w^* = L_w^*/U_0^* = 0.27s$ with a randomized initial position and zero initial velocity. It is assumed that the vortex length scale $\hat{L}_w$ to estimate is a constant within the range from a lower bound $L_{lb} = 1m$ to an upper bound $L_{ub} = 12m$. The incremental length scale dL is chosen to be $0.2m$. As shown in Fig. 1, the estimated vortex length scale with the highest weight is $\hat{L}_w = 4.20m$. The corresponding estimated mean velocity is $\hat{U}_0 = 15.95m/s$, and the resultant estimated vortex time scale is $\hat{\tau}_w = \hat{L}_w/\hat{U}_0 = 0.26s$. All three estimated cellular flow parameters are close to their true values. Table 1 shows that, with reasonable restrictions on the range of L_{cand} and careful choice of incremental length scale dL, the cellular flow parameters U_0, L_w and τ_w can be estimated accurately within a range of error around ±4% for this simulation.

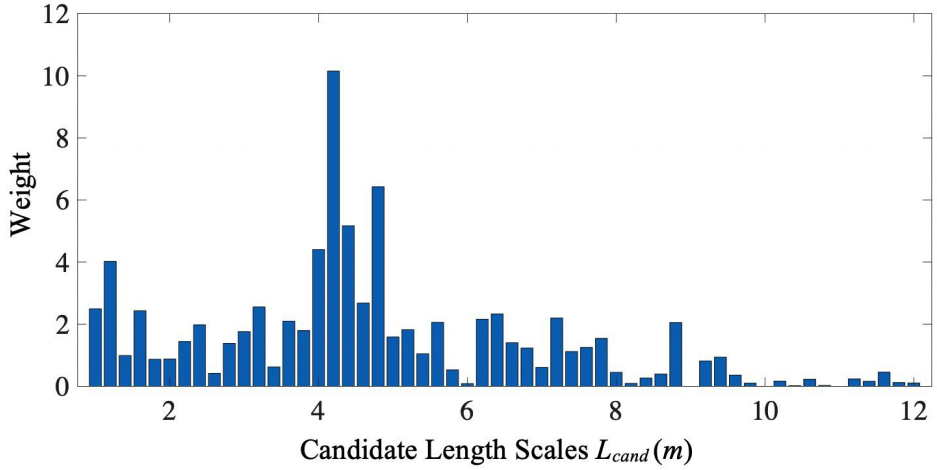

Fig. 1 Weights of the candidate length scales L_{cand} ranging from a lower bound $L_{lb} = 1m$ to an upper bound $L_{ub} = 12m$. The estimated vortex length scale with the highest weight is $\hat{L}_w = 4.20m$.

To evaluate the overall performance, the parameter estimation algorithms are then validated on simulated thrust-driven air vehicles with different initial conditions traversing cellular flows with different parameters. Among 95 measurement data sets, the vortex timescale τ_w^* of the cellular flow is equally spaced within the range from $0.05s$ to $1s$, and the vortex length scale L_w^* is a random number. Additionally, the vehicle's initial position is randomized, and its initial velocity

Table 1 Comparison of the true and estimated values of the cellular flow parameters.

	$U_0(m/s)$	$L_w(m)$	$\tau_w(s)$
True Value	15.43	4.21	0.27
Estimated Value	15.95	4.20	0.26
Percentage Error	3.37%	-0.24%	-3.70%

is set to zero. The overall performance is shown in Fig. 2. At most times, the vortex timescale $\hat{\tau}_w$, the vortex length scale $\hat{L}_w$ and the mean velocity $\hat{U}_0$ can be estimated accurately with a few outliers arising possibly due to measurement noise and inaccuracy caused by estimating the state derivatives via finite difference approximation. Furthermore, when testing the algorithms on simulated data sets with smaller vortex timescales τ_w^*, the deviations of the estimated vortex length scales $\hat{L}_w$ and mean velocities $\hat{U}_0$ from their true values increase. However, some data points in Fig. 2 show that deviated estimations of the vortex length scale $\hat{L}_w$ and mean velocity $\hat{U}_0$ are correlated so that their ratio yields relatively good estimations of the vortex timescale $\hat{\tau}_w$. With 95 different simulations and validation tests, the average absolute errors and percentage errors of the three cellular flow parameters are listed in Table 2 below. After comparing their average percentage errors, we draw the conclusion that the parameter estimation algorithms proposed in this paper can estimate the vortex length scale $\hat{L}_w$ more accurately than the vortex timescale $\hat{\tau}_w$ and mean velocity $\hat{U}_0$.

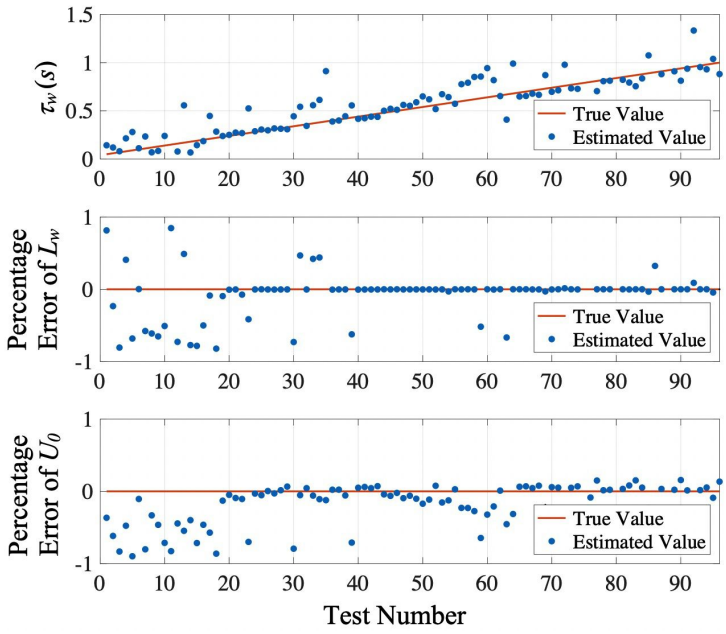

Fig. 2 Overall performance of the parameter estimation algorithms on different simulated data sets. In general, the vortex timescale $\hat{\tau}_w$, the vortex length scale $\hat{L}_w$ and the mean velocity $\hat{U}_0$ can be accurately estimated with only a few outliers arising.

Table 2 Average absolute and percentage errors of the three cellular flow parameters.

	$U_0(m/s)$	$L_w(m)$	$\tau_w(s)$
Absolute Error	-4.43	-0.17	0.10
Percentage Error	-18.80%	-5.91%	33.30%

VII. Conclusions and Future Work

With reasonable restrictions on the range of vortex length scales L_w and an appropriate incremental length scale dL, the vortex timescale τ_w can be estimated accurately within a permissible range of error by the proposed methods. However, when testing the parameter estimation algorithms on different simulated data sets, we observe that small errors in the estimated vortex length scale $\hat{L}_w$ can make the algorithms unable to distinguish one ultimate candidate function from others, thus resulting in dispersed weights and a large deviation when estimating the mean velocity $\hat{U}_0$ and the vortex timescale $\hat{\tau}_w$. Errors in the estimated vortex length scales $\hat{L}_w$ may be caused by the low resolution and inappropriate choice of the incremental length scale dL when constructing the library of all potential candidate functions. Regarding future work beyond the ideal point-mass thrust-driven air vehicle model and cellular flow model described here, the proposed flow parameter estimation algorithms can be extended to more complicated air vehicle models, such as fixed-wing aircraft and quadcopters, and to turbulent flow models, such as k-epsilon (k-ε) turbulence models and Reynolds-stress models (RSM).

Acknowledgments

This work is supported by the Office of Naval Research grant N00014-17-1-2614.

References

[1] Aliseda, A., Cartellier, A., Hainaux, F., and Lasheras, J. C., "Effect of preferential concentration on the settling velocity of heavy particles in homogeneous isotropic turbulence," *Journal of Fluid Mechanics*, Vol. 468, 2002, pp. 77–105.

[2] Good, G., Ireland, P., Bewley, G., Bodenschatz, E., Collins, L., and Warhaft, Z., "Settling regimes of inertial particles in isotropic turbulence," *Journal of Fluid Mechanics*, Vol. 759, 2014.

[3] Yang, H., Bewley, G., and Ferrari, S., "Flow-aided Vehicle Navigation and Control in Turbulence," *AIAA Journal*, to be submitted.

[4] Bollt, S. A., and Bewley, G. P., "How to Extract Energy from Turbulence in Flight by Fast Tracking," *under review*, 2020.

[5] Xiang, X., Wang, Z., Mo, Z., Chen, G., Pham, K., and Blasch, E., "Wind field estimation through autonomous quadcopter avionics," *2016 IEEE/AIAA 35th Digital Avionics Systems Conference (DASC)*, IEEE, 2016, pp. 1–6.

[6] Garau, B., Alvarez, A., and Oliver, G., "AUV navigation through turbulent ocean environments supported by onboard H-ADCP," *Proceedings 2006 IEEE International Conference on Robotics and Automation, 2006. ICRA 2006.*, IEEE, 2006, pp. 3556–3561.

[7] Langelaan, J. W., Alley, N., and Neidhoefer, J., "Wind field estimation for small unmanned aerial vehicles," *Journal of Guidance, Control, and Dynamics*, Vol. 34, No. 4, 2011, pp. 1016–1030.

[8] Randeni, P., Supun, A., Forrest, A. L., Cossu, R., Leong, Z. Q., Ranmuthugala, D., et al., "Determining the horizontal and vertical water velocity components of a turbulent water column using the motion response of an autonomous underwater vehicle," *Journal of Marine Science and Engineering*, Vol. 5, No. 3, 2017, p. 25.

[9] Song, Z., and Mohseni, K., "FACON: A flow-aided cooperative navigation scheme," *2017 IEEE/RSJ International Conference on Intelligent Robots and Systems (IROS)*, IEEE, 2017, pp. 6251–6256.

[10] MahmoudZadeh, S., Powers, D., Sammut, K., and Yazdani, A., "Differential evolution for efficient AUV path planning in time variant uncertain underwater environment," *Robotics (cs. RO)*, 2016.

[11] Waslander, S., and Wang, C., "Wind disturbance estimation and rejection for quadrotor position control," *AIAA Infotech@ Aerospace conference and AIAA unmanned... Unlimited conference*, 2009, p. 1983.

[12] Hayes, D. R., and Morison, J. H., "Determining turbulent vertical velocity, and fluxes of heat and salt with an autonomous underwater vehicle," *Journal of Atmospheric and Oceanic Technology*, Vol. 19, No. 5, 2002, pp. 759–779.

[13] Levine, E. R., and Lueck, R. G., "Turbulence measurement from an autonomous underwater vehicle," *Journal of atmospheric and oceanic technology*, Vol. 16, No. 11, 1999, pp. 1533–1544.

[14] Pope, S. B., "Turbulent flows," , 2001.

[15] Kaiser, E., Kutz, J. N., and Brunton, S. L., "Sparse identification of nonlinear dynamics for model predictive control in the low-data limit," *Proceedings of the Royal Society A*, Vol. 474, No. 2219, 2018, p. 20180335.

[16] Brunton, S. L., Proctor, J. L., and Kutz, J. N., "Discovering governing equations from data by sparse identification of nonlinear dynamical systems," *Proceedings of the national academy of sciences*, Vol. 113, No. 15, 2016, pp. 3932–3937.

[17] Lorenz, E. N., "Deterministic nonperiodic flow," *Journal of the atmospheric sciences*, Vol. 20, No. 2, 1963, pp. 130–141.

[18] Noack, B. R., Afanasiev, K., MORZYŃSKI, M., Tadmor, G., and Thiele, F., "A hierarchy of low-dimensional models for the transient and post-transient cylinder wake," *Journal of Fluid Mechanics*, Vol. 497, 2003, pp. 335–363.

[19] Maxey, M., and Corrsin, S., "Gravitational settling of aerosol particles in randomly oriented cellular flow fields," *Journal of the atmospheric sciences*, Vol. 43, No. 11, 1986, pp. 1112–1134.

[20] Langmuir, I., "Surface motion of water induced by wind," *Science*, Vol. 87, No. 2250, 1938, pp. 119–123.

[21] Stommel, H., "Trajectories of small bodies sinking slowly through convection cells," *J. mar. Res*, Vol. 8, No. 11, 1949, pp. 24–29.

[22] Chung, T. H., Clement, M. R., Day, M. A., Jones, K. D., Davis, D., and Jones, M., "Live-fly, large-scale field experimentation for large numbers of fixed-wing UAVs," *2016 IEEE International Conference on Robotics and Automation (ICRA)*, IEEE, 2016, pp. 1255–1262.

[23] Hauert, S., Leven, S., Varga, M., Ruini, F., Cangelosi, A., Zufferey, J.-C., and Floreano, D., "Reynolds flocking in reality with fixed-wing robots: communication range vs. maximum turning rate," *2011 IEEE/RSJ International Conference on Intelligent Robots and Systems*, IEEE, 2011, pp. 5015–5020.

[24] Preiss, J. A., Honig, W., Sukhatme, G. S., and Ayanian, N., "Crazyswarm: A large nano-quadcopter swarm," *2017 IEEE International Conference on Robotics and Automation (ICRA)*, IEEE, 2017, pp. 3299–3304.

[25] Preiss, J. A., Hönig, W., Ayanian, N., and Sukhatme, G. S., "Downwash-aware trajectory planning for large quadrotor teams," *2017 IEEE/RSJ International Conference on Intelligent Robots and Systems (IROS)*, IEEE, 2017, pp. 250–257.

[26] Barnes, L., Fields, M., and Valavanis, K., "Unmanned ground vehicle swarm formation control using potential fields," *2007 Mediterranean Conference on Control & Automation*, IEEE, 2007, pp. 1–8.

[27] Siegwart, R., Nourbakhsh, I. R., and Scaramuzza, D., *Introduction to autonomous mobile robots*, MIT press, 2011.

[28] Maxey, M., "The gravitational settling of aerosol particles in homogeneous turbulence and random flow fields," *Journal of Fluid Mechanics*, Vol. 174, 1987, pp. 441–465.